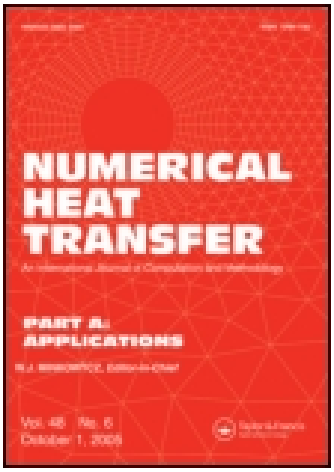

Numerical Heat Transfer, Part A: Applications: An International Journal of Computation and Methodology
Publication details, including instructions for authors and subscription information:
http://www.tandfonline.com/loi/unht20

Transient Laminar MHD Natural Convection Cooling in a Vertical Cylinder

A. J. Iatridis [a] , C. D. Dritselis [a] , I. E. Sarris [b] & N. S. Vlachos [a]
[a] Department of Mechanical Engineering , University of Thessaly, Athens Avenue , Volos , Greece
[b] Department of Energy Technology , Technological & Educational Institution of Athens , Egaleo , Greece
Published online: 27 Sep 2012.

To cite this article: A. J. Iatridis , C. D. Dritselis , I. E. Sarris & N. S. Vlachos (2012) Transient Laminar MHD Natural Convection Cooling in a Vertical Cylinder, Numerical Heat Transfer, Part A: Applications: An International Journal of Computation and Methodology, 62:7, 531-546, DOI: 10.1080/10407782.2012.703082

To link to this article: http://dx.doi.org/10.1080/10407782.2012.703082

Numerical Heat Transfer, Part A, 62: 531–546, 2012

ISSN: 1040-7782 print/1521-0634 online
DOI: 10.1080/10407782.2012.703082

Taylor & Francis
Taylor & Francis Group

TRANSIENT LAMINAR MHD NATURAL CONVECTION COOLING IN A VERTICAL CYLINDER

A. J. Iatridis[1], C. D. Dritselis[1], I. E. Sarris[2], and N. S. Vlachos[1]

[1]*Department of Mechanical Engineering, University of Thessaly, Athens Avenue, Volos, Greece*

[2]*Department of Energy Technology, Technological & Educational Institution of Athens, Egaleo, Greece*

A numerical study is presented of transient laminar natural convection cooling of an electrically conductive fluid, placed in a vertical cylinder in the presence of an axial magnetic field. The cylindrical wall is suddenly cooled to a uniform temperature, thus setting the fluid to motion. The cooling process starts with the development of momentum and thermal boundary layers along the cylindrical cold wall, followed by the intrusion of the cooled fluid into the bulk, and finally, by fluid stratification. A range of Hartmann, Rayleigh, and Prandtl numbers are studied for which the flow remains laminar in all stages. It is found that the increase of the magnetic field reduces the heat transfer rate and decelerates the cooling process. This can be attributed to the damping of the fluid motion by the magnetic field, which results in the domination of conduction over convection heat transfer. The increase of the Rayleigh number enhances heat transfer, but the cooling process lasts longer due to the higher temperature of the hot fluid. The flow deceleration and the reduction of heat transfer are less intense for fluids with low Prandtl number.

1. INTRODUCTION

Natural convection cooling, frequently occurring in environmental flows and in engineering applications, has recently received considerable attention because of the need to increase heat transfer rates without the penalty of increased pumping power. For example, Papanicolaou and Belessiotis [1] studied heat transfer in a cylindrical water tank, while Lee and Hyun [2] investigated the stratification in thermosyphon and air systems in the presence of both electromagnetic and buoyancy forces. The transient cooling of the fluid in a cylindrical container with a

Received 28 October 2011; accepted 18 May 2012.

This work was performed in the framework of the Association EURATOM — Hellenic Republic and is supported by the European Union within the Fusion Program. A. J. Iatridis is thankful for a doctoral scholarship, and C. D. Dritselis for a postdoctoral fellowship from the Association. The content of this article is the sole responsibility of the authors and it does not necessarily represent the views of the Commission or its services.

Address correspondence to N. S. Vlachos, Laboratory of Fluid Mechanics and Turbomachinary, Department of Mechanical and Industrial Engineering, University of Thessaly, Athens Avenue, 38334 Volos, Greece. E-mail: vlachos@mie.uth.gr

NOMENCLATURE

B_0	magnitude of magnetic field, T	T_w	constant wall temperature, K
c_p	fluid specific heat, $J\,kg^{-1}\,K^{-1}$	u_0	free fall velocity $(g\beta H\Delta T)^{1/2}$, ms^{-1}
D	diameter of cylindrical container, m	u_r	radial velocity, ms^{-1}
g	gravity acceleration, ms^{-2}	U_r	dimensionless radial velocity, u_r/u_0
H	height of cylindrical container, m	u_z	axial velocity, ms^{-1}
Ha	Hartmann number, $Ha = B_0 H\sqrt{\frac{\sigma}{\rho\nu}}$	U_z	dimensionless axial velocity, u_z/u_0
k	fluid thermal conductivity, $Wm^{-1}\,K^{-1}$	z	axial coordinate
Nu	average Nusselt number	Z	dimensionless axial coordinate, z/H
p	pressure, Pa	α	fluid thermal diffusivity, m^2s^{-1}
P	dimensionless pressure, $\frac{p}{\rho u_0^2}$	β	fluid thermal expansion coefficient, K^{-1}
Pr	Prandtl number, $Pr = \frac{\nu}{\alpha}$	ΔT	temperature difference $T_0 - T_w$, K
r	radial coordinate	θ	dimensionless temperature, $(T - T_0)/(T_0 - T_w)$
R	dimensionless radial coordinate, r/H	θ_α	dimensionless average temperature
Ra	Rayleigh number, $Ra = \frac{g\beta H^3\Delta T}{\nu\alpha}$	μ	fluid dynamic viscosity, $kg\,m^{-1}s^{-1}$
T	temperature, K	ν	fluid kinematic viscosity, $m^2\,s^{-1}$
t	time, s	ρ	fluid density, $kg\,m^{-3}$
t	dimensionless time, tu_0/H	σ	fluid electrical conductivity, Sm^{-1}
T_0	initial temperature, K	Ψ	dimensionless streamfunction

suddenly cooled wall has no statistical stationarity, except at the two limiting motionless states of $t = 0$ and $t \to \infty$. This is in contrast to other natural convection configurations such as, for example, Rayleigh-Bérnard convection [3] or laterally and volumetrically heated enclosures [4]. Lin and Armfield [5] and Hyun [6] showed that the cooling process starts with the development of momentum and thermal boundary layers on the cool cylindrical wall. This stage is followed by the intrusion of cold fluid into the bulk hot fluid from the bottom corner of the cylinder. Finally, the flow and the temperature fields are stratified and the fluid is cooled-down to a uniform lower temperature, which is determined by the imposed thermal boundary conditions.

Bouabdallah et al. [7] studied numerically the phase change of molten gallium in three-dimensional oscillatory natural convection flow in a parallelepiped enclosure in the presence of an external magnetic field. They found that the magnetic field stabilized the oscillatory natural convection, producing two-dimensional flow and thermal characteristics. Öğüt [8] studied the MHD flow and heat transfer due to natural convection in a square enclosure with a finite length heater. The effects of the heater length and location, magnetic force direction, and Hartmann and Grashof numbers were examined. It was found that heat transfer is reduced with an increasing Hartmann number. The Grashof number affects the rate of the reduction, with its increase resulting in a higher rate of reduction of heat transfer. A numerical study of the external magnetic field effect on the laminar free convection was carried out by Sarris et al. [9]. The magnetic forcing controls the flow, and strong magnetic fields may even reverse the usual convection currents. High Hartmann numbers or low Reynolds numbers can cause an increase of the intensity of the flow circulation and heat transfer of the sidewalls. The latter can rise up to 40%, depending on the combination of the magnetic and gravitational forces.

In their three-dimensional numerical study of a flow in a rectangular enclosure, under the existence of an external magnetic field, Battira and Bessaïh [10] concluded that the flow control can be accomplished by the proper selection of strength and direction of the magnetic field and the electric conductivity. The vertical magnetic field results in a stronger decrease of the fluid motion than the horizontal one. Furthermore, the thermal stratification in the core is destroyed and the isotherms are parallel to the vertical walls. Bessaïh and Bouabdallah [11] investigated numerically the two-dimensional, oscillatory natural convection of a liquid metal solidification in a rectangular cavity in the presence of an external magnetic field. They showed that the vertical magnetic field stabilized the convection flow and they provided diagrams with dependencies of the critical Grashof numbers and frequencies on the magnetic field. The buoyant MHD flow of an electrically conducting, internally heated fluid in a vertical square duct was studied by Sposito and Ciofalo [12]. Recirculation occurred for intermediate values of pressure gradient and mean velocity. Velocity and electric potential upper limits were found for Hartmann numbers above 100.

Most previous studies aimed at investigating the natural convection cooling of fluids with Prandtl numbers (Pr) higher than unity. However, the cooling process of fluids with low Pr is also of great interest; for example, in the flooding of the reactor cavity of nuclear power plants in case of an accident [13]. Hyun [14] studied the effect of the Prandtl number on the fluid heating-up. Also, the cooling process of a low Prandtl number fluid in a vertical cylinder [15] or in a rectangular vertical container [16, 17] was studied numerically, providing scaling laws.

Recently, Sarris et al. [18] studied numerically the transient turbulent cooling of a liquid-metal (i.e., a very low Prandtl number fluid) in the presence of an external magnetic field. It was observed that the magnetic field does not significantly affect the initial stage of the boundary layer development, while it decelerates heat transfer during the thermal intrusion of the cold fluid into the bulk. However, at the final stage of thermal stratification, the cooling process is decelerated by the magnetic field for low Rayleigh numbers, while it is accelerated for higher ones.

Flow and heat transfer can be affected by applying an external magnetic field as, for example, in the case of metal casting, and in the breeding/cooling blanket of future fusion devices where very high magnetic fields are applied to confine the plasma. The present flow configuration relates to cases of accidents in nuclear reactors and also to fusion reaction heat removal in fusion blankets. In the present study, the interest is focused mostly on the effect of a constant axial magnetic field on the transient laminar cooling of a low-Pr fluid in a vertical cylinder. The parametric study includes several combinations of Hartmann, Prandtl, and Rayleigh numbers in the laminar flow regime.

For the same configuration, Sarris et al. [18] studied combinations of these numbers that led to turbulence. To the best knowledge of the authors, this is the first attempt to study the transient laminar MHD cooling of a low-Pr fluid in a vertical cylindrical container. Thus, this study contributes to a better understanding of how the cooling process of low-Pr fluids is affected by a uniform magnetic field. The present results are also of practical interest in the design and development of liquid-metal heat exchangers (e.g., blankets) for future fusion reactors.

2. PROBLEM DEFINITION

2.1. Flow Configuration

The present flow configuration consists of an electrically conductive fluid, initially at rest in a vertical cylindrical container of height H, diameter D, and a fixed aspect ratio $D/H = 2$, as shown in Figure 1. The top and bottom horizontal walls are adiabatic, while all walls are electrically insulated. Initially, the fluid is at uniform temperature T_0, and, suddenly, the cylindrical wall is cooled to a constant temperature $T_w < T_0$, while a vertical (axial) magnetic field of magnitude B_0 is applied externally.

2.2. Governing Equations

The governing equations of the present axisymmetric thermally driven flow are the mass continuity equation, the incompressible Navier-Stokes momentum equations, and the energy conservation equation.

$$\frac{1}{r}\frac{\partial(ru_r)}{\partial r} + \frac{\partial(u_z)}{\partial z} = 0 \tag{1}$$

$$\rho\left(\frac{\partial u_r}{\partial \tau} + \frac{1}{r}\frac{\partial(ru_r u_r)}{\partial r} + \frac{\partial(u_z u_r)}{\partial z}\right) = -\frac{\partial p}{\partial r} + \mu\left(\frac{\partial}{\partial r}\left(\frac{1}{r}\frac{\partial(ru_r)}{r\partial r}\right) + \frac{\partial^2 u_r}{\partial z^2}\right) - \sigma u_r B_0^2 \tag{2}$$

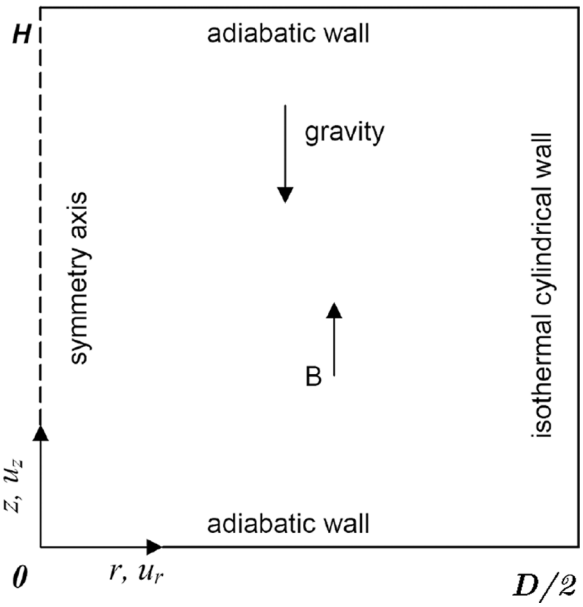

Figure 1. Flow geometry and boundary conditions.

$$\rho\left(\frac{\partial u_z}{\partial \tau}+\frac{1}{r}\frac{\partial (ru_ru_z)}{\partial r}+\frac{\partial (u_zu_z)}{\partial z}\right)=-\frac{\partial p}{\partial z}+\mu\left(\frac{\partial}{\partial r}\left(\frac{1}{r}\frac{\partial ru_z}{\partial r}\right)+\frac{\partial^2 u_z}{\partial z^2}\right)+\rho g\beta(T-T_0) \quad (3)$$

$$\rho c_p\left(\frac{\partial T}{\partial \tau}+\frac{1}{r}\frac{\partial (ru_rT)}{\partial r}+\frac{\partial (u_zT)}{\partial z}\right)=k\left(\frac{\partial}{\partial r}(\frac{1}{r}\frac{\partial rT}{\partial r})+\frac{\partial^2 T}{\partial z^2}\right) \quad (4)$$

where p is the total pressure, u_r and u_z are the radial and axial fluid velocity components, respectively, r and z are the radial and axial coordinates, respectively, τ is the time, T is the fluid temperature, T_0 is the initial uniform fluid temperature, μ is the fluid viscosity, ρ its density, c_p its specific heat, σ its electrical conductivity, β its thermal expansion, k its thermal conductivity, B_0 is the magnitude of the external axial magnetic field, and g is the acceleration due to gravity.

The Boussinesq approximation for the buoyancy term has been used in Eq. (3), while the effect of the constant axial magnetic field on the fluid is represented by the Lorentz force in Eq. (2) based on the low magnetic Reynolds number approximation [19]. In this approximation, the induced magnetic field is considered very weak as compared to the external magnetic field B_0, which is generally true for low magnetic Reynolds number flows as those of liquid-metals and electrolytes in laboratory experiments. A useful discussion for the validity limits of this approximation for natural convection flows can be found in Sarris et al. [20]. The effects of viscous dissipation and Joule heating on the present flow are considered negligible.

The above equations are made nondimensional by using the height of the cylinder H, the temperature difference $\Delta T = T_0 - T_w$, the amplitude of the external magnetic field B_0, and the free fall velocity $u_0 = (g\beta H\Delta T)^{1/2}$.

$$\frac{1}{R}\frac{\partial (RU_r)}{\partial R}+\frac{\partial U_z}{\partial Z}=0 \quad (5)$$

$$\frac{\partial U_r}{\partial t}+\frac{\partial (RU_rU_r)}{R\partial R}+\frac{\partial (U_zU_r)}{\partial Z}=-\frac{\partial P}{\partial R}+\left(\frac{\mathrm{Pr}}{\mathrm{Ra}}\right)^{\frac{1}{2}}\left\{\frac{\partial}{\partial R}\left(\frac{1}{R}\frac{\partial (RU_r)}{\partial R}\right)+\frac{\partial^2 U_r}{\partial Z^2}\right\} - \mathrm{Ha}^2\left(\frac{\mathrm{Pr}}{\mathrm{Ra}}\right)^{\frac{1}{2}}U_r \quad (6)$$

$$\frac{\partial U_z}{\partial t}+\frac{\partial (RU_rU_z)}{R\partial R}+\frac{\partial (U_zU_z)}{\partial Z}=-\frac{\partial P}{\partial Z}+\left(\frac{\mathrm{Pr}}{\mathrm{Ra}}\right)^{\frac{1}{2}}\left\{\frac{\partial}{\partial R}\left(\frac{1}{R}\frac{\partial RU_z}{\partial R}\right)+\frac{\partial^2 U_z}{\partial Z^2}\right\}+\theta \quad (7)$$

$$\frac{\partial \theta}{\partial t}+\frac{1}{R}\frac{\partial (RU_r\theta)}{\partial R}+\frac{\partial (U_z\theta)}{\partial Z}=\frac{1}{(\mathrm{RaPr})^{\frac{1}{2}}}\left[\frac{\partial}{\partial R}\left(\frac{1}{R}\frac{\partial R\theta}{\partial R}\right)+\frac{\partial^2 \theta}{\partial Z^2}\right] \quad (8)$$

where $P = p/(\rho u_0^2)$ is the dimensionless pressure, $U_r = u_r/u_0$ and $U_z = u_z/u_0$ are the dimensionless radial and axial fluid velocity components, respectively, $R = r/H$ and $Z = z/H$ are the dimensionless radial and axial coordinates, respectively,

$t = \tau u_0/H$ is the dimensionless time, and finally, the dimensionless temperature is defined as $\theta = (T - T_0)/(T_0 - T_w)$.

The present flow is characterized by three-dimensionless parameters: the Rayleigh number (Ra), the Prandtl number (Pr) and the Hartmann number (Ha), defined as follows.

$$\mathrm{Ra} = \frac{g\beta H^3 \Delta T}{\nu\alpha}, \quad \mathrm{Pr} = \frac{\nu}{\alpha}, \quad \mathrm{Ha} = B_0 H \sqrt{\frac{\sigma}{\rho\nu}} \tag{9}$$

where ν is the kinematic viscosity and α the thermal diffusivity of the fluid.

For the range of parameters studied here, the axial magnetic field has no significant impact on the axisymmetry of the present flow. The axisymmetry of this flow has also been demonstrated in the case of a cylindrical container with an applied sinusoidal temperature on its upper lid by Kakarantzas et al. [21]. However, this is not true for other configurations, as for example, in homogeneous turbulence or an horizontal magnetic field [22].

The initial and boundary conditions are as follows.

$$\text{For } t \leq 0: \; U_r = U_z = \theta = 0 \tag{10}$$

$$\text{For } t > 0: \; U_r = U_z = 0, \frac{\partial \theta}{\partial Z} = 0 \;\text{ for } Z = 0 \text{ and } 1 \tag{11}$$

$$U_r = 0, \frac{\partial U_z}{\partial R} = \frac{\partial \theta}{\partial R} = 0 \;\text{ for } R = 0 \tag{12}$$

$$U_r = U_z = 0, \; \theta = -1, \;\text{ for } R = 1 \tag{13}$$

An instantaneous Nusselt number averaged on the isothermal cylindrical wall is calculated as follows.

$$\mathrm{Nu} = \int_0^1 \left(-\frac{\partial \theta}{\partial R} \right)_{R=1} dZ \tag{14}$$

A streamfunction Ψ is calculated from the velocity field using the following.

$$U_r = \partial \Psi / \partial Z \tag{15}$$

A measure of the average nondimensional bulk fluid temperature is as follows.

$$\theta_\alpha = \int_0^1 \int_0^1 \theta \, dR \, dZ \tag{16}$$

where initially (i.e., $t \leq 0$) $\theta_\alpha = 0$.

2.3. Numerical Method and Simulation Details

The governing equations are solved by the use of a CFD code developed in-house [18]. A staggered mesh and a second-order accurate finite differencing scheme are used for the discretization of the nondimensional governing equations (5)–(8), as suggested by Verzicco and Orlandi [23]. The final system of algebraic equations is solved with a fractional step method. The time integration of the diffusion terms is performed by a Crank-Nicolson method, while a third-order Runge-Kutta method is used for the nonlinear terms, the buoyancy term, and the Lorentz force. Mass continuity is enforced by solving a Poisson equation for the pseudopressure [23, 24], based on the FISHPACK library [25].

A nonuniform grid based on hyperbolic tangent distribution functions was used for both the axial and radial directions in order to resolve the boundary layers on the horizontal top and bottom walls, and on the vertical cylindrical wall as well as near the symmetry axis, based on the considerations of Lin and Armfield [5, 26] and Sarris et al. [18].

A grid independence test showed that a mesh size of 200×200 and a time step of $\Delta t = 2.5 \times 10^{-5}$ were adequate to fully resolve the flow characteristics, while the use of finer meshes did not affect significantly the results. The present numerical model has been validated successfully against the results of Lin and Armfield [15] (see for more details Sarris et al. [18]).

3. RESULTS AND DISCUSSION

Direct numerical simulations were performed using fluids with $\mathrm{Pr} = 0.03$, 0.1, and 0.7. The parametric study involved three Rayleigh numbers: $\mathrm{Ra} = 10^4$, 10^5 and 10^6, and four Hartmann numbers: $\mathrm{Ha} = 0$, 25, 50, and 100. Combinations of these parameters were carefully selected to ensure that the flow always remains laminar.

The effect of magnetic field on the streamfunction and isotherms at times $t = 1$, 3, 5, 10, and 20 during the transient cooling process is illustrated in Figures 2 and 3, respectively. In particular, Figure 2 shows the distribution of the streamfunction for combinations of $\mathrm{Pr} = 0.03$, 0.7, $\mathrm{Ra} = 10^4$, 10^6, and $\mathrm{Ha} = 0$, 100. It is found that there is only a small influence of the magnetic field on the flow and the cooling process for $t \leq 1$. However, for $t > 1$, it can be seen that the flow is suppressed by the magnetic field resulting in a recirculation zone narrower in the radial direction. The deceleration of the fluid by the damping action of the magnetic field is more pronounced for the higher Pr fluid with increasing Ra, as it may be seen by the comparison of Figures 2*a* and 2*b* ($\mathrm{Pr} = 0.03$) with Figures 2*c* and 2d ($\mathrm{Pr} = 0.7$), respectively. In the hydrodynamic case ($\mathrm{Ha} = 0$) and for high Ra values, the strong convective currents lead to a second recirculation for $t > 10$, especially for the low-Pr fluid. In the presence of the magnetic field with $\mathrm{Ha} = 100$, this second pattern is not observed and the time evolution of the streamfunction is qualitatively similar to that of the lower Ha cases, yielding more noticeable differences for the higher Ra between the MHD and the non-MHD cases.

Figure 3 shows the isotherms corresponding to the streamfunction distributions of Figure 2. During the first stage of the cooling process, the development of the vertical thermal layer occurs, which seems to be little affected by the magnetic

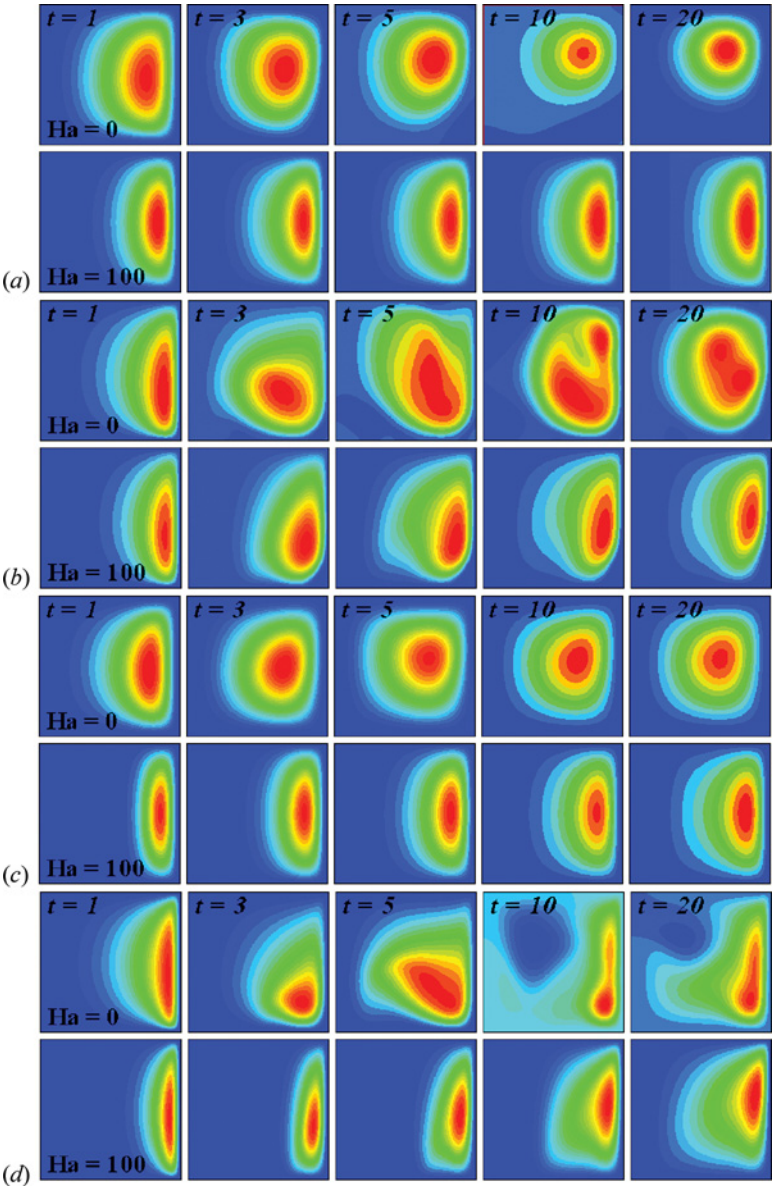

Figure 2. Streamfunction distributions in the initial cooling stage for Ha = 0 (upper) and Ha = 100 (lower) at (*a*) Pr = 0.03, Ra = 10^4, (*b*) Pr = 0.03, Ra = 10^6, (*c*) Pr = 0.7, Ra = 10^4, and (*d*) Pr = 0.7, Ra = 10^6. The minimum, increment and maximum contour values are 0, 0.002 and 0.038, respectively (color figure available online).

field for all values of Ra, Pr, and Ha studied. Without the magnetic field, the penetration of the cold fluid to the hotter bulk for Ra = 10^4 is mostly made by conduction for $t \leq 1$, while the fluid motions are strong enough to mix and cool the bulk fluid for $t > 1$. The fluid velocities are attenuated by the magnetic field resulting in a

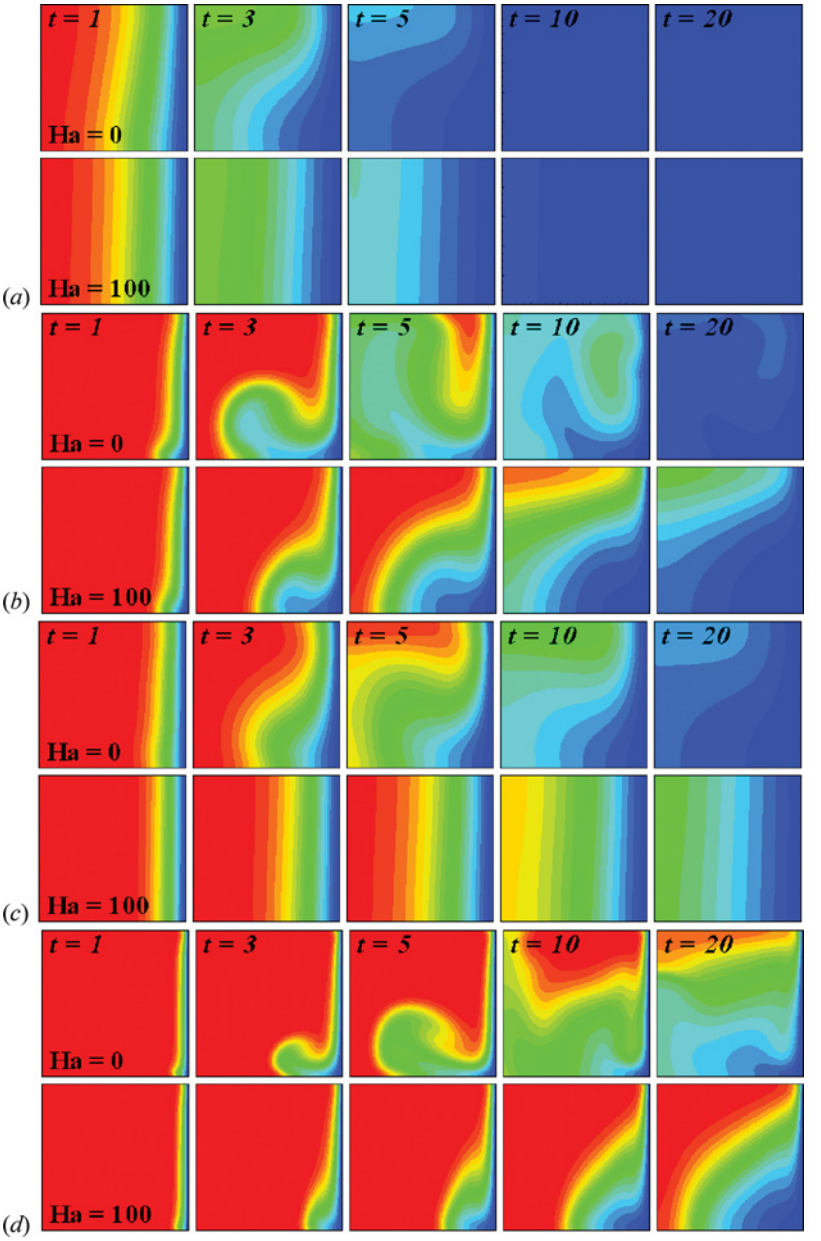

Figure 3. Temperature distributions in the initial cooling stage for Ha = 0 (upper) and Ha = 100 (lower). (*a*) Pr = 0.03, Ra = 10^4, (*b*) Pr = 0.03, Ra = 10^6, (*c*) Pr = 0.7, Ra = 10^4, and (*d*) Pr = 0.7, Ra = 10^6. The minimum, increment and maximum contour values are −0.95, −0.05 and −0.05, respectively (color figure available online).

delay of the cooling process. This behavior is also observed in all other cases examined. A considerable delay of the cooling is evident in the stages of the intrusion of cold fluid and stratification as compared with the pure hydrodynamic case, which is

more pronounced with increasing Ra and for the higher-Pr fluids, as indicated in Figure 3. The main observation is that the flow is damped by the magnetic field, leading to a situation where conduction prevails over convection and, thus, reducing heat transfer. A greater percentage of the vessel contains fluid of higher temperature and, consequently, more time is required to cool the fluid in the presence of the magnetic field.

The dimensionless thickness δ_θ of the thermal boundary layer developing on the cylindrical wall is shown in Figure 4 for $\mathrm{Pr} = 0.03$ and 0.7, $\mathrm{Ha} = 0$ to 100, and $\mathrm{Ra} = 10^4$ and 10^6. This thickness is defined as the radial distance from the cylindrical wall where the fluid temperature reaches $0.01(T_w - T_0)$. For time $t \leq 1$, the thickness of the thermal boundary layer is similar for all Hartmann numbers examined, revealing a small impact of the magnetic field during the initial cooling stage. At the higher Rayleigh number of 10^6, it is seen that more time is required for the thermal boundary layer to become fully developed with increasing Ha, while an insignificant influence of the magnetic field is observed at the lower Rayleigh number of 10^4. The vertical thermal boundary layer acquires its maximum thickness at shorter times with decreasing Ra and Pr numbers. This is true for the case $\mathrm{Ra} = 10^4$, $\mathrm{Pr} = 0.03$ (not shown here), irrespective of the magnitude of the magnetic field. Consequently, as the Prandtl number is increased, the thermal boundary layer appears to be thinner at the same time for all values of Hartmann number studied.

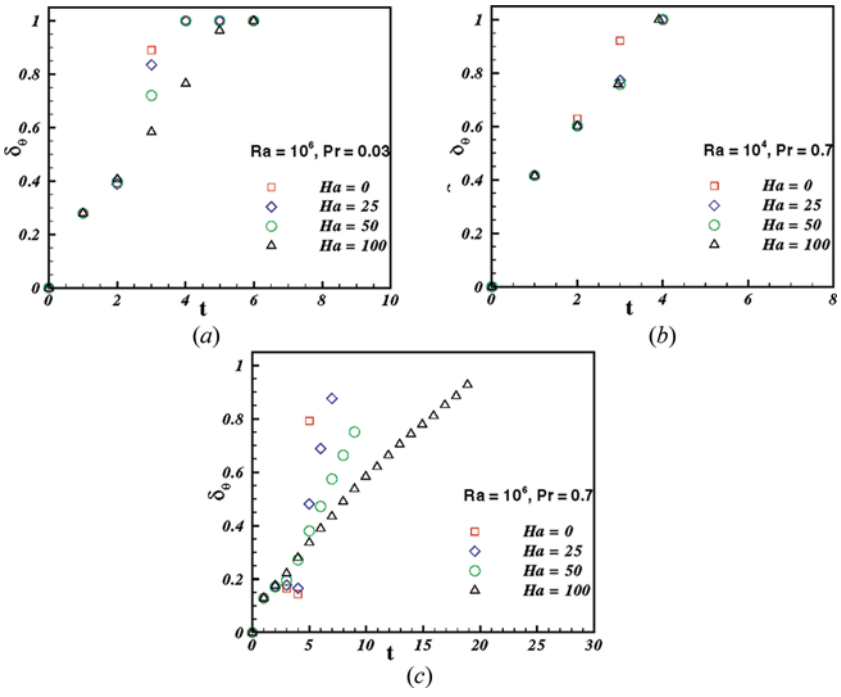

Figure 4. Variation of the thickness of the vertical thermal boundary layer for various Hartmann numbers: (*a*) $\mathrm{Pr} = 0.03$, $\mathrm{Ra} = 10^6$, (*b*) $\mathrm{Pr} = 0.7$, $\mathrm{Ra} = 10^4$, and (*c*) $\mathrm{Pr} = 0.7$, $\mathrm{Ra} = 10^6$ (color figure available online).

Figure 4*c* shows that the boundary layer is suppressed for $t < 5$ and $\mathrm{Ha} = 0$, while it is thickened again for $t \geq 5$. This can be attributed to the fact that at the start of the flow development along the cylindrical wall, the fluid at the bottom moves upwards into the bulk and against the cylindrical wall, resulting in suppression of the boundary layer in accordance with the findings of reference [18]. With time passing, the side wall flow acquires enough momentum to resist the bulk flow. The same observation occurs for all the cases with the magnetic field, even for $\mathrm{Ha} = 100$ to a much lesser degree. This means that the magnetic field helps the vertical thermal boundary layer to grow into the initial resting bulk fluid due to the damping of the upward fluid motion near the bottom of the container. This is true for the higher Ra and Pr studied, while for the lower value of Pr or Ra, shown in Figures 4*a* and 4*b*, respectively, the development of the vertical boundary layer is not decreased, meaning that it is not suppressed by the bulk flow. The above result is supported by Figure 2*d* at $t = 3$, which shows the flow being suppressed for $\mathrm{Ha} = 0$ or $\mathrm{Ha} = 100$. At $t = 3$ the circulation region gets thinner and for $t = 5$ it starts growing, while the bulk flow delays the growth of the boundary layer. In the case of $\mathrm{Ha} = 100$ this bulk flow is smaller and weaker, while the fluid remains hot in the center of the bottom wall. The isotherms of Figure 3*d* for the same case show the expansion of the center bulk flow at $t = 5$ for $\mathrm{Ha} = 0$, while for $\mathrm{Ha} = 100$ this expansion is lesser, not being able to affect the boundary layer thickness.

Figure 5 shows the thickness of the thermal boundary layer as a function of $(\mathrm{RaPr})^{-1/4}$ for Hartmann numbers of $\mathrm{Ha} = 0$, 25, 50, and 100 at times $t = 1$ and 3. It is evident that the magnetic field has no significant effect on the early stage of cooling at $t = 1$. However, at time $t = 3$ the cooling process is affected by the magnetic field and depending on the value of $(\mathrm{RaPr})^{-1/4}$, the cooling process is

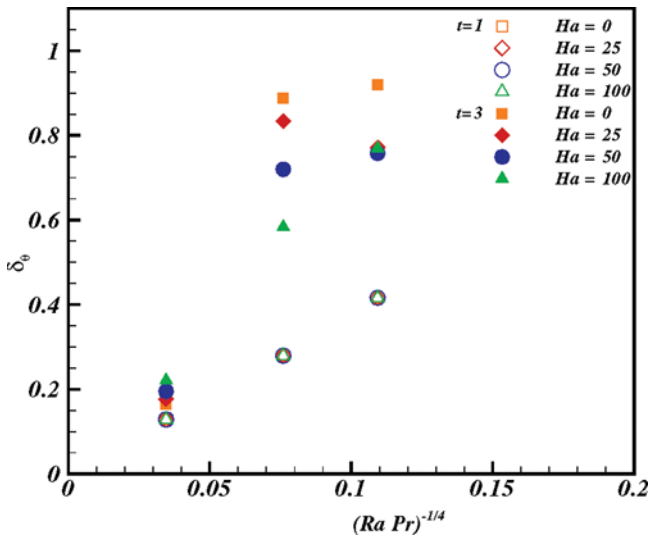

Figure 5. Variation of the thermal boundary layer thickness at various Hartmann numbers scaled with $(\mathrm{RaPr})^{-1/4}$ (color figure available online).

affected by the magnetic field. Similar results have been obtained for $\mathrm{Pr} = 0.1$ and $\mathrm{Ra} = 10^5$, but are not shown here for brevity.

Figure 6 shows the time variation of the Nusselt number for different Hartmann numbers and for $\mathrm{Pr} = 0.03$, 0.1, 0.7 and $\mathrm{Ra} = 10^4$, 10^5, 10^6. The most important observation is that the heat transfer is decreased with increasing Hartmann number for all values of Pr and Ra studied. The observed enhancement of heat transfer with increasing Rayleigh number can be attributed to the larger temperature differences between the hot bulk fluid and the cold wall. However, the cooling process lasts longer as indicated by the increase of the time period required to reduce the values of Nu to zero, which corresponds to the final motionless state. Similarly, larger values of Nu and a longer cooling process are found for the higher Pr fluid. Figure 6 shows that there is a time period in which the values of Nu in the MHD cases are smaller than that of the hydrodynamic case, while the opposite is observed for larger times. The low values of the Nusselt numbers denote that the heat transfer is decreased due to the flow deceleration by the magnetic field. For $\mathrm{Ra} = 10^4$ and $\mathrm{Pr} = 0.03$, the Nusselt number is decreased for $t \leq 5$ while it is increased for $t > 5$ with increasing Ha. The time for which the value of Nu starts to increase with Ha is changed depending on the Prandtl and Rayleigh numbers. For example, for $\mathrm{Pr} = 0.7$ this time is $t = 12$ at $\mathrm{Ra} = 10^4$, while it becomes approximately 33 at $\mathrm{Ra} = 10^6$. During the thermal stratification stage, the Nusselt number is not affected significantly by the

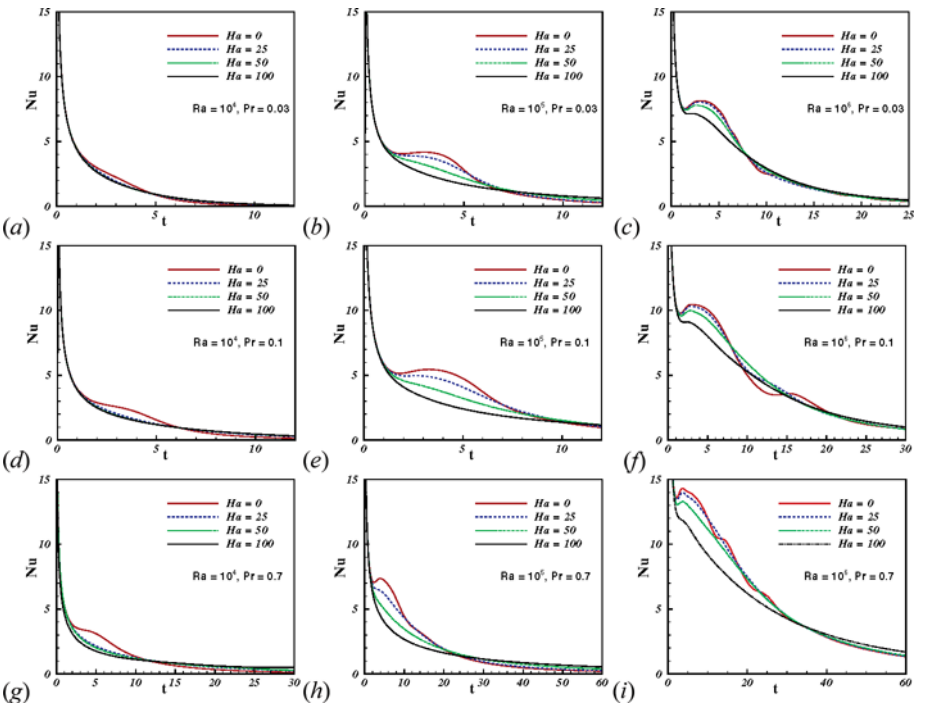

Figure 6. Time variation of Nusselt number at different Hartmann numbers: $\mathrm{Pr} = 0.03$ (upper), $\mathrm{Pr} = 0.1$ (middle), $\mathrm{Pr} = 0.7$ (lower), $\mathrm{Ra} = 10^4$ (left), $\mathrm{Ra} = 10^5$ (middle), and $\mathrm{Ra} = 10^6$ (right) (color figure available online).

magnetic field, mainly because of the weak fluid motion due to the small temperature differences in the bulk fluid.

A good indicator of the rate of cooling is the average fluid temperature, θ_a (Lin and Armfield [5, 26] and Sarris et al. [18]). Figure 7 shows the temporal variation of θ_a for various combinations of Prandtl, Rayleigh, and Hartmann numbers. For low Ra and Pr values, it seems that during the initial cooling stage the average fluid temperature θ_a in the MHD cases does not differ much from that in the hydrodynamic case. During the intrusion of the cold fluid into the bulk, the cooling process is delayed and longer times are required to decrease θ_a for fluids with high Prandtl number. It is obvious from Figure 7 that for high Prandtl, Rayleigh and Hartmann numbers, the temperature of the fluid remains higher for longer time periods. Consequently, the slope of the curves of θ_a is less steep, indicating generally more time to cool the fluid in these cases.

Figure 8 shows the radial distribution of temperature at the level $z = H/2$ at various times in the presence of magnetic field with $\mathrm{Ha} = 100$, for $\mathrm{Pr} = 0.03$, 0.7, and $\mathrm{Ra} = 10^4$, 10^6. It can be seen that the rate of temperature reduction depends on Ra and Pr, consistent with the observations in Figure 3. It is evident that this reduction is also a function of the radial position r. For example, the temperature is decreased more in the central region of the vessel for $\mathrm{Ra} = 10^4$ and $\mathrm{Pr} = 0.03$, while the temperature is reduced mainly near the cylindrical wall for $\mathrm{Ra} = 10^6$ and $\mathrm{Pr} = 0.7$.

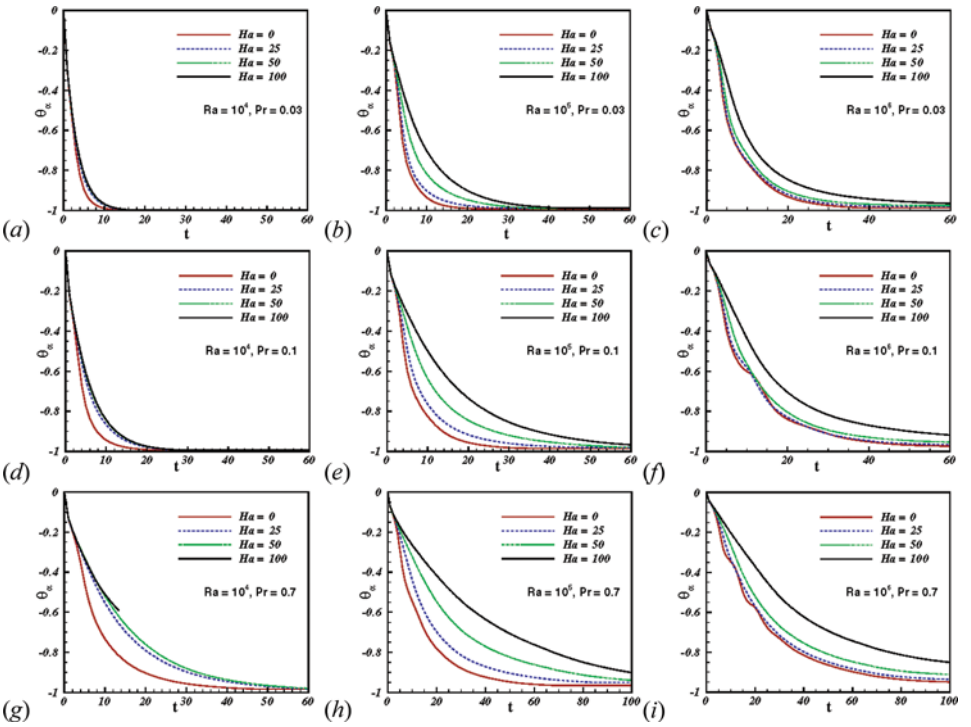

Figure 7. Time evolution of average temperature at various Hartmann numbers: $\mathrm{Pr} = 0.03$ (upper), $\mathrm{Pr} = 0.1$ (middle), $\mathrm{Pr} = 0.7$ (lower), $\mathrm{Ra} = 10^4$ (left), $\mathrm{Ra} = 10^5$ (middle), $\mathrm{Ra} = 10^6$ (right) (color figure available online).

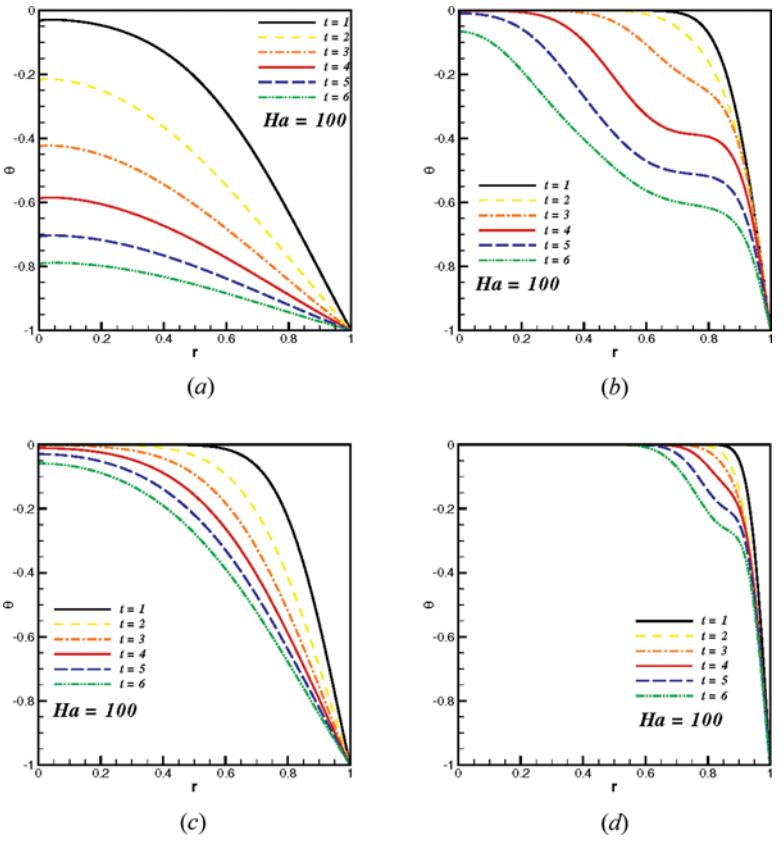

Figure 8. Radial distribution of temperature at $z = H/2$ for $\mathrm{Ha} = 100$. (*a*) $\mathrm{Pr} = 0.03$, $\mathrm{Ra} = 10^4$, (*b*) $\mathrm{Pr} = 0.03$, $\mathrm{Ra} = 10^6$, (*c*) $\mathrm{Pr} = 0.7$, $\mathrm{Ra} = 10^4$, and (*d*) $\mathrm{Pr} = 0.7$, $\mathrm{Ra} = 10^6$ (color figure available online).

In addition, it is clear that the temperature distribution near the cylindrical wall is steeper for fluids with lower Prandtl numbers. Qualitatively, similar observations can also be made for all other cases examined in the present study.

4. CONCLUSION

The present numerical study was focused on the effect of an axial magnetic field on the transient laminar natural convection cooling of a low-Prandtl number hot fluid contained in a cold vertical cylinder. Direct numerical simulations were carried out for different values of Prandtl, Rayleigh, and Hartmann numbers at which the flow remained always laminar. It was shown that in the presence of the magnetic field, the fluid motion is damped resulting to a deceleration of fluid cooling.

The magnetic field has little influence on the initial stage of boundary layer development on the cylindrical wall. The vertical thermal boundary layer becomes fully developed very quickly at times that are independent of Hartmann number for low Prandtl and Rayleigh numbers, while longer times are generally required

with increasing Hartmann number for large Prandtl and Rayleigh numbers. For large values of Pr and Ra, the cold fluid intrudes from the vertical to the bottom wall and, finally, to the bulk fluid through the central vessel area, opposing the development of the thermal boundary layer on the sidewall. Due to the damping action of the magnetic field, the cold fluid intrusion is significantly diminished and the thermal stratification is delayed with increasing Ha. Consequently, conduction dominates over convection and heat transfer is reduced, which is more pronounced for high Prandtl and Rayleigh numbers. A larger percentage of the cylinder remains at higher temperature and, thus, the cooling process lasts longer relative to the pure hydrodynamic case. Finally, the presence of the magnetic field does not play a great role during the ending of the fluid stratification process.

REFERENCES

1. E. Papanicolaou and V. Belessiotis, Transient Natural Convection in a Cylindrical Enclosure at High Rayleigh Numbers, *Int. J. Heat and Mass Transfer*, vol. 45 no. 7, pp. 1425–1444, 2002.
2. S. H. Lee and J. M. Hyun, Transient Buoyant Convection of Air in an Enclosure under Strong Magnetic Effect, *Int. J. Heat and Mass Transfer*, vol. 8, no. 15, pp. 3097–3106, 2005.
3. R. Verzicco and R. Camussi, Numerical Experiments on Strongly Turbulent Thermal Convection in a Slender Cylindrical Cell, *J. Fluid Mechanics*, vol. 477, pp. 19–49, 2003.
4. I. E. Sarris, S. C. Kakarantzas, A. P. Grecos, and N. S. Vlachos, MHD Natural Convection in a Laterally and Volumetrically Heated Square Cavity, *Int. J. Heat and Mass Transfer*, vol. 48, pp. 3443–3453, 2005.
5. W. Lin and S. W. Armfield, Natural Convection Cooling of Rectangular and Cylindrical Containers, *Int. J. Heat and Fluid Flow*, vol. 22, no. 1, pp. 72–81, 2001.
6. J. M. Hyun, Unsteady Buoyancy Convection in an Enclosure, *Adv. Heat Transfer*, vol. 24, pp. 277–320, 1994.
7. S. Bouabdallah, R. Bessaïh, B. Ghernaout, and A. Benchatti, Effect of an External Magnetic Field on the 3-D Oscillatory Natural Convection of Molten Gallium during Phase Change, *Numer. Heat Transfer: A*, vol. 60, pp. 84–105, 2011.
8. E. B. Ögüt, Magnetohydrodynamic Natural Convection Flow in an Enclosure with a Finite Length Heater using the Differential Quadrature (DQ) Method, *Numer. Heat Transfer: A*, vol. 58, pp. 900–921, 2010.
9. I. E. Sarris, D. G. E. Grigoriadis, and N. S. Vlachos, Laminar free Convection in a Square Enclosure Driven by the Lorentz Force, *Numer. Heat Transfer: A*, vol. 58, pp. 923–942, 2010.
10. M. Battira and R. Bessaïh, Three-Dimensional Natural Convection in the Horizontal Bridgman Configuration under Various Wall Electrical Conductivity and Magnetic Field, *Numer. Heat Transfer: A*, vol. 55, pp. 58–76, 2009.
11. R. Bessaïh and S. Bouabdallah, Numerical Study of Oscillatory Natural Convection during Solidification of a Liquid Metal in a Rectangular enclosure with and without Magnetic Field, *Numer. Heat Transfer: A*, vol. 54, no. 3, pp. 331–348, 2008.
12. G. Sposito and M. Ciofalo, Fully Developed Mixed Magnetohydrodynamic Convection in a Vertical Square Duct, *Numer. Heat Transfer: A*, vol. 53, no. 9, pp. 907–924, 2008.
13. R. R. Nourgaliev, T. N. Dinh, and B. R. Sehgal, Simulation and Analysis of Transient Cooldown Natural Convection Experiments, *Nuclear Eng. and Design*, vol. 178, no. 1, pp. 13–27, 1997.

14. J. M. Hyun, Effect of the Prandtl Number on Heat-Up of a Stratified Fluid in an Enclosure, *ASME J. Heat Transfer*, vol. 107, pp. 982–984, 1985.
15. W. Lin and S. W. Armfield, Scaling Laws for Unsteady Natural Convection Cooling of Fluid with Prandtl Number Less than one in a Vertical Cylinder, *Physical Revi. E*, vol. 72, pp. 016–306, 2005.
16. W. Lin, S. W. Armfield, and J. C. Patterson, Cooling of a $Pr < 1$ Fluid in a Rectangular Container, *J. Fluid Mechanics*, vol. 574, pp. 85–108, 2007.
17. W. Lin and S. W. Armfield, Long-Term Behavior of Cooling Fluid in a Vertical Cylinder, *Int. J. Heat and Mass Transfer*, vol. 48, pp. 53–66, 2005.
18. I. E. Sarris, A. I. Iatridis, C. D. Dritselis, and N. S. Vlachos, Magnetic Field Effect on the Cooling of a Low-Pr Fluid in a Vertical Cylinder, *Physics of Fluids*, vol. 22, pp. 017–101, 2010.
19. R. Moreau, *Magnetohydrodynamics*, Kluwer Academic Press, London, 1998.
20. I. E. Sarris, G. K. Zikos, A. P. Grecos, and N. S. Vlachos, On the Limits of Validity of the Low Magnetic Reynolds Number Approximation in MHD Natural Convection Heat Transfer, *Numer. Heat Transfer: B*, vol. 50, pp. 157–180, 2006.
21. S. C. Kakarantzas, I. E. Sarris, A. P. Grecos, and N. S. Vlachos, Magnetohydrodynamic Natural Convection in a Sinusoidal Upper Heated Cylindrical Cavity, *Int. J. Heat and Mass Transfer*, vol. 52, pp. 250–259, 2009.
22. S. C. Kakarantzas, A. P. Grecos, N. S. Vlachos, I. E. Sarris, B. Knaepen, and D. Carati, Direct Numerical Simulation of a Heat Removal Configuration for Fusion Blankets, *Energy Conversion and Management*, vol. 48, pp. 2775–2783, 2007.
23. R. Verzicco and P. Orlandi, A Finite-Difference Scheme for Three-Dimensional Incompressible flow in Cylindrical Coordinates, *J. Computational Physics*, vol. 123, pp. 402–414, 1996.
24. P. Orlandi, *Fluid Flow Phenomena: A Numerical Toolkit*, Kluwer Academic Press, London, 2001.
25. P. Swarztrauber and R. Sweet, *Efficient FORTRAN Subprograms for the Solution of Elliptic Partial Differential Equations*, NCAR Technical Note-TN/IA-109, (1975).
26. W. Lin and S. W. Armfield, Direct Simulation of Natural Convection Cooling in a Vertical Circular Cylinder, *Int. J. Heat and Mass Transfer*, vol. 42, pp. 4117–4130, 1999.